Stabilizing a single-magnon state by optimizing magnon blockade

Zhu-yao Jin and Jun Jing*
School of Physics, Zhejiang University, Hangzhou 310027, Zhejiang, China

(Received 23 April 2024; accepted 10 July 2024; published 24 July 2024)

A stable and high-quality single-magnon state is desired by the single-magnon source for quantum-information application with a macroscopic spin system. We consider a hybrid system where a magnon mode is directly coupled to a nonresonant superconducting qubit via the exchange interaction. The magnon and qubit are under the driving and probing fields with the same frequency, respectively. We find that the single-magnon probability P_1 can be maximized when the product of the magnon-driving field detuning and the qubit-probing field detuning is equivalent to the square of the magnon-qubit coupling strength, $\Delta_q\Delta_m \approx J^2$. Then, the double-magnon probability P_2 can be minimized by tuning the ratio of the probing intensity to the driving intensity and the relative phase between the two fields. Under these optimized conditions with accessible strong driving intensity and low decay rate, strong magnon blockade gives rise to a stable single-magnon state with a high quality. It features a large brightness (the single-magnon probability) $P_1 \approx 0.40$ and a high purity (the equal-time second-order correlation function) $g^{(2)}(0) \sim 10^{-5}$. The two indicators as a whole prevail over the existing results for photon, phonon, and magnon modes with respect to a stable single-quantum state. The optimized conditions with a scalable modification $\Delta_q\Delta_m \approx NJ^2$ apply to the situation when one focuses on any one of the N magnon modes that are simultaneously coupled to a common qubit.

DOI: 10.1103/PhysRevA.110.012459

I. INTRODUCTION

As a quantized spin wave, magnon can be generated by the collective excitation of a large number of spins in the yttrium iron garnet (YIG) sphere [1–3], a ferrimagnetic insulator with an extremely high spin density and record low damping rate. Recently, the YIG sphere [1] becomes an essential component of various hybrid magnonic systems that have attracted considerable attention in advancing quantum information processing [4,5] and quantum technology [6]. At least two reasons support that the hybrid magnonic systems are more promising than the optomechanical systems: (1) by virtue of the great tunability in frequency [2,7–10], magnons can be integrated with plentiful quantum elements, including phonon modes [11–13], microwave photons [7–10,14–17], optical photons [18–22], and superconducting qubits [23–28], by various coupling schemes such as pressure-like interaction and magnetic dipole interaction [29]; (2) owing to the high spin density of YIG, strong [8–10,15] or even ultrastrong interaction [14,16,17] between a magnon and a microwave cavity, and strong indirect [23–27] (mediated by a microwave cavity) or strong direct interactions [28] between a magnon and a superconducting qubit have been established. One can thus exploit magnons, the macroscopic spin system, to carry out diversified tasks of information processing in both classical and quantum regimes.

A lot of exotic properties of the hybrid magnonic systems have been detected in the classical regime, such as bistability [30,31], multistability [32], magnonic frequency comb [33–35], and magnonic Penrose superradiance [35]. In the quantum regime, many proposals were put forward to generate entangled states, such as entangling the magnon-photon-phonon system [12,36], generating the Bell states between a magnon and photon [37,38], and entangling two magnons through a microwave cavity [39–41]. Other applications include quantum transducer [42,43] and quantum sensing [27,44,45]. The quantum control over the macroscopic spin system [25,26] is fundamentally based on the operation at the level of a single magnon, similar to that over the superconducting resonator [46], the optomechanical resonator [47,48], and the acoustic-wave systems [49]. From the ground state, the magnon Fock states and their superposition [50–53] can be nondeterministically heralded or temporarily generated through direct or indirect exchange interaction.

In the long-time limit, a single-magnon state could be stabilized by magnon blockade [54–58], working as a solid-state single-quantum resource. Similar to the single-photon source [59], by which a single photon can be emitted at the moments desired by the user [60], the steady single-magnon state relies on optimized blockade conditions and is irrelevant to the initial state. Enlightened by the statistics in a photon or phonon blockade [59,61–70], the steady single-magnon state is characterized with a significant occupation on the single-quantum state P_1 and a low equal-time second-order correlation function $g^{(2)}(0)$. The standard criterion for confirming a steady single-magnon state is $g^{(2)}(0) < 0.5$ [68], since $g^{(2)}(0) = 0.5$ when the magnon is at the Fock state $|2\rangle$. A perfect Fock state $|1\rangle$ [68] implies that $P_1 \to 1$ and $g^{(2)}(0) \to 0$. However, most existing proposals focus only on optimizing the $g^{(2)}$ function, and the magnitude of P_1 is typically in the range of $(0.01, 0.1)$.

*Contact author: jingjun@zju.edu.cn

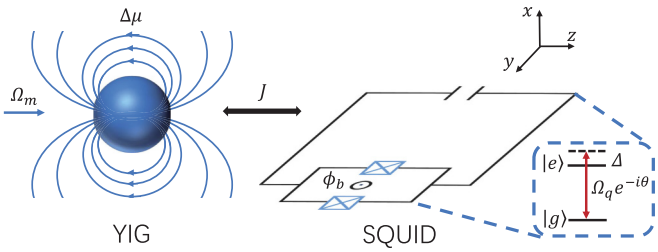

FIG. 1. Sketch of the hybrid magnon-qubit system, in which the ferromagnetic YIG sphere is directly coupled to a superconducting transmon qubit [28]. The magnon and the qubit are, respectively, under the driving field with Rabi frequency Ω_m and the probing field with Rabi frequency Ω_q. The two fields are out of phase with θ.

In this paper, we are motivated to prepare a stable and high-quality single-magnon state by optimizing magnon blockade in a system where the magnon is coupled to a nonresonant superconducting qubit via the exchange interaction [28]. In particular, we seek to amplify the single-magnon probability P_1 and suppress the double-magnon probability P_2 when the system is pushed to the strong blockade regime. The optimized conditions are confirmed to be associated with the qubit-probing field detuning, magnon-driving field detuning, magnon-qubit coupling strength, field intensity ratio, and the relative phase between the two fields. Using the fact that P_1 is roughly proportional to the driving-field intensity and inversely proportional to the system decay rate, one can achieve $P_1 \sim 0.40$ and $g^{(2)}(0) \sim 10^{-5}$ with the achievable parameters. In regard to the two indicators, the best and balanced results for a steady single-photon state are found to be $P_1 \sim 0.10$ and $g^{(2)}(0) \sim 10^{-2}$, which were constructed by a two-photon absorption process of the environment [71]. Straightforwardly, our proposal can be generalized to a model of N magnons coupled to a common qubit [72–74], in which every magnon mode can be stabilized as a high-quality single-excitation resource under the scaled condition for maximizing P_1.

The rest of this paper is structured as follows. In Sec. II, we introduce the hybrid magnon-qubit system under the external driving and probing fields. In Sec. III A, we use an approximate model with a non-Hermitian Hamiltonian to analytically derive the optimal conditions for the strong magnon blockade, and they are numerically confirmed in Sec. III B. Next, in Sec. III C, we approach the high-quality and stable single-magnon state through numerical optimization. In Sec. IV, we discuss the general case with N magnons. The whole work is concluded in Sec. V.

II. MODEL AND HAMILTONIAN

We consider a hybrid magnon-qubit system [28] as shown in Fig. 1, where a YIG sphere is directly coupled to a superconducting transmon qubit via the transversal (exchange) interaction J. The original Hamiltonian reads ($\hbar \equiv 1$)

$$H = \omega_q \sigma_+ \sigma_- + \omega_m m^\dagger m + J(m\sigma_+ + m^\dagger \sigma_-). \tag{1}$$

The qubit is formed by a superconducting quantum interference device (SQUID) loop and a capacitor in parallel. And, the SQUID loop is interrupted by two Josephson junctions. The flux through the SQUID loop consists of the external flux Φ_b induced by the control lines carrying direct and alternating currents and the flux $\Phi(\Delta\mu)$ caused by the magnetic fluctuation $\Delta\mu$. The latter establishes the direct magnon-qubit interaction, including the transversal and longitudinal parts. The transversal part follows the exchange interaction form [23,75], which plays a key role in our proposal. And, the longitudinal interaction is analogous to the radiation pressure in optomechanics [76–78]. Both of them can be tuned through modulating the external flux Φ_b and the magnon-qubit distance d. When the external flux $\Phi_b/\Phi_0 \approx 0.5$ (Φ_0 is the magnetic flux quantum) [28], the longitudinal interaction can be switched off. In this situation, the transversal interaction can be tuned up to about $J/2\pi \sim 35$ MHz [28] by properly positioning the magnon and qubit. As for the indirect coupling mediated by the cavity [23–26], the magnon-qubit exchange interaction is about $J/2\pi \sim 15$ MHz. The qubit frequency $\omega_q/2\pi$ is tunable in the range from 1 to 10 GHz through modulating the external flux Φ_b and the SQUID asymmetry α [28], e.g., $\omega_q/2\pi \sim 1.5$ GHz for $\Phi_b/\Phi_0 \approx 0.5$ and $\alpha = 0.01$. In comparison to its optomechanical counterpart [61,79], the magnon frequency $\omega_m = \gamma B$ with γ the gyromagnetic ratio is flexibly tunable in the range of 1–10 GHz through the external bias magnetic field B. In terms of the Gilbert damping constant $\alpha_G \sim 10^{-5} - 10^{-4}$ [28], the damping rate of magnon $\kappa_m/2\pi \sim \omega_m \alpha_G$ is on the order of 0.1–1 MHz [10,28].

To push the magnon mode into the single-quantum state through magnon blockade, the qubit and magnon are respectively driven by a probing field and a driving field, which are assumed to be resonant in frequency ω. Typically, ω is on the order of gigahertz [30]. We consider a relative phase θ between the probing and driving fields. Then, the total Hamiltonian becomes

$$\begin{aligned} H_{\rm tot} = {} & \omega_q \sigma_+ \sigma_- + \omega_m m^\dagger m + J(m\sigma_+ + m^\dagger \sigma_-) \\ & + \left[\Omega_m m^\dagger e^{-i\omega t} + \Omega_q \sigma_+ e^{-i(\omega t+\theta)} + \text{H.c.}\right], \end{aligned} \tag{2}$$

where the probing intensity $\Omega_q = k\sqrt{P_d}$ with $k = 103\,\text{MHz/mW}^{1/2}$ [80] and a field power P_d as strong as 350 mW [30], and the driving intensity $\Omega_m = \sqrt{2S}\Omega_s$ with S the total spin number of the macroscopic spin system and Ω_s the coupling strength of the driving field with the macrospin [81]. In the rotating frame with respect to $H' = \omega(m^\dagger m + \sigma_+ \sigma_-)$, the effective Hamiltonian reads

$$\begin{aligned} H_{\rm eff} = {} & \Delta_q \sigma_+ \sigma_- + \Delta_m m^\dagger m + J(m\sigma_+ + m^\dagger \sigma_-) \\ & + \Omega_m(m^\dagger + m) + \Omega_q(\sigma_+ e^{-i\theta} + \sigma_- e^{i\theta}), \end{aligned} \tag{3}$$

where $\Delta_q \equiv \omega_q - \omega$ and $\Delta_m \equiv \omega_m - \omega$. Here, we consider a more general situation than the existing proposals [54,64,67,82] where the magnon and qubit are nonresonant, i.e., $\Delta_q \neq \Delta_m$.

III. OPTIMAL CONDITIONS FOR STABILIZING SINGLE-MAGNON STATE

A. Maximize single-magnon probability

Statistically, the single-magnon state could be characterized with brightness and purity. The former is defined as the

average occupation

$$\bar{n} = \langle m^\dagger m\rangle = \sum_{n>0} nP_n \tag{4}$$

with the probability in the magnon-number state

$$P_n \equiv \langle n|\rho_m|n\rangle, \tag{5}$$

and the latter is suggested by the equal-time second-order correlation function [83,84]

$$g^{(2)}(0) = \frac{\langle m^\dagger m^\dagger m m\rangle}{\langle m^\dagger m\rangle^2}. \tag{6}$$

Here, the expectation values are evaluated by the reduced density matrix for the magnon mode ρ_m, which can be obtained by partially tracing the full density matrix ρ of the steady state over the degree of freedom of the qubit.

When the magnon is pushed to the blockade regime with a strong antibunching effect, $g^{(2)}(0) \to 0$, i.e., $P_0, P_1 \gg \sum_n P_{n>1}$ and $P_2 \gg P_{n>2}$, the brightness of the single-magnon state becomes

$$\bar{n} \approx P_1, \tag{7}$$

and the purity can be expressed by

$$g^{(2)}(0) = \frac{\sum_{n=2}^{\infty} n(n-1)P_n}{\sum_{n=1}^{\infty}(nP_n)^2} \approx \frac{2P_2}{P_1^2}. \tag{8}$$

In the strong-coupling limit, i.e., $J \gg \Omega_m, \Omega_q$, an analytical model [54–57,63–66] can be used to estimate the wave function of the composite system and then to derive analytically the optimal conditions for amplifying P_1 and suppressing P_2. Despite the fact that this model cannot be fully correct in the presence of dissipation, the resulting optimal conditions for P_1 and P_2 can be confirmed with the master-equation approach [63]. Specifically, the system dynamics can be approximately determined by the non-Hermitian Hamiltonian

$$H_{\rm non} = H_{\rm eff} - i\frac{\kappa}{2}(\sigma_+\sigma_- + m^\dagger m) \tag{9}$$

with the effective Hamiltonian $H_{\rm eff}$ in Eq. (3). And, the composite system could be truncated to a subspace with a few excitations (not greater than two), i.e., the system evolution can be approximately described by

$$|\psi\rangle = C_{g0}|g0\rangle + C_{g1}|g1\rangle + C_{e0}|e0\rangle + C_{e1}|e1\rangle + C_{g2}|g2\rangle, \tag{10}$$

where C_α ($\alpha = g0, g1, e0, e1, g2$) is the probability amplitude and $|g(e)\rangle$ and $|n\rangle$ denote the ground (excited) state of qubit and the Fock state of the magnon mode, respectively. Then, the relevant dynamical equations can be written as

$$\begin{aligned}
i\dot{C}_{e0} &= JC_{g1} + \Omega_q e^{-i\theta}C_{g0} + \tilde{\Delta}_q C_{e0},\\
i\dot{C}_{g1} &= JC_{e0} + \Omega_m C_{g0} + \tilde{\Delta}_m C_{g1},\\
i\dot{C}_{e1} &= \sqrt{2}JC_{g2} + \Omega_q e^{-i\theta}C_{g1} + \Omega_m C_{e0} + (\tilde{\Delta}_q + \tilde{\Delta}_m)C_{e1},\\
i\dot{C}_{g2} &= \sqrt{2}JC_{e1} + \sqrt{2}\Omega_m C_{g1} + 2\tilde{\Delta}_m C_{g2},
\end{aligned} \tag{11}$$

where $\tilde{\Delta}_{q,m} \equiv \Delta_{q,m} - i\kappa/2$. The steady-state solutions yield

$$C_{g1} = \frac{J\Omega_q e^{-i\theta} - \Omega_m\tilde{\Delta}_q}{\tilde{\Delta}_q\tilde{\Delta}_m - J^2}, \tag{12a}$$

$$C_{g2} = \frac{\sqrt{2}(AC_{g1} - B)}{2\tilde{\Delta}_m(\tilde{\Delta}_q + \tilde{\Delta}_m) - 2J^2} \tag{12b}$$

$$C_{e1} = \frac{-\sqrt{2}J\tilde{\Delta}_q C_{g2} - (\Omega_q\tilde{\Delta}_q e^{-i\theta} - \Omega_m J)C_{g1}}{\tilde{\Delta}_q(\tilde{\Delta}_q + \tilde{\Delta}_m)} + \frac{B}{J(\tilde{\Delta}_q + \tilde{\Delta}_m)} \tag{12c}$$

with the coefficients A and B

$$\begin{aligned}
A &= J\Omega_q e^{-i\theta} - \left(\tilde{\Delta}_q + \tilde{\Delta}_m + \frac{J^2}{\tilde{\Delta}_q}\right)\Omega_m,\\
B &= \frac{J\Omega_m\Omega_q e^{-i\theta}}{\tilde{\Delta}_q}.
\end{aligned} \tag{13}$$

The single-magnon and double-magnon probabilities can thus be expressed as

$$\begin{aligned}
P_1 &= |C_{g1}|^2 + |C_{e1}|^2 \approx |C_{g1}|^2,\\
P_2 &= |C_{g2}|^2
\end{aligned} \tag{14}$$

under the approximation $|C_{g1}| \gg |C_{e1}|$. In the weak decay regime, i.e., $\kappa \ll \Delta_{m,q}, J$, the population on the state $|g1\rangle$ can be maximized by

$$\Delta_q\Delta_m \approx \tilde{\Delta}_q\tilde{\Delta}_m = J^2 \tag{15}$$

due to Eq. (12a). Then, the amplitude magnitude $|C_{g2}|$ in Eq. (12b) can be optimized by minimizing the coefficient A for C_{g1}. With Eq. (13), Eq. (15), and $\theta \ll 1$, the condition reads

$$\frac{\Omega_q}{\Omega_m} \approx \frac{\Delta_q + 2\Delta_m}{J}. \tag{16}$$

Consequently, we have

$$C_{g2} \approx \frac{i\sqrt{2}[4\Delta_m(\Delta_q + 2\Delta_m)\theta - (\Delta_q + 7\Delta_m)\kappa]\Omega_m^2}{2\Delta_m^2(\Delta_q + \Delta_m)\kappa}, \tag{17}$$

by which $|C_{g2}|$ can be further reduced if

$$\theta \to \theta_{\rm opt} = \frac{(\Delta_q + 7\Delta_m)\kappa}{4\Delta_m(\Delta_q + 2\Delta_m)}. \tag{18}$$

B. Numerical verification of optimal conditions

We here numerically verify the optimal conditions presented in Eqs. (15), (16), and (18) for the strong magnon blockade. The first condition primarily targets increasing the single-magnon occupation P_1, and the second and third one contribute to decreasing the double-magnon occupation P_2 as well as the equal-time second-order correlation function $g^{(2)}(0)$.

The decoherence dynamics toward the steady state can be calculated by the master equation [83],

$$\frac{\partial}{\partial t}\rho = -i[H_{\rm eff}, \rho] + \frac{\kappa_m}{2}\mathcal{L}_m[\rho] + \frac{\kappa_q}{2}\mathcal{L}_{\sigma_-}[\rho], \tag{19}$$

where $H_{\rm eff}$ is the effective Hamiltonian in Eq. (3) and the dissipator is defined as the Lindblad superoperators

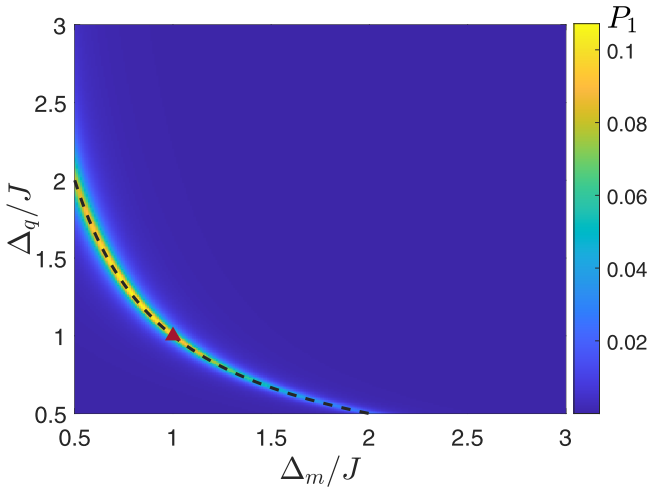

FIG. 2. Single-magnon probability P_1 vs the ratio of the detuning Δ_q to the coupling strength J and the ratio of the detuning Δ_m to the coupling strength J. The black dashed line follows the optimal condition about $\Delta_q\Delta_m$ in Eq. (15). The red triangle describes the resonant case $\Delta_q = \Delta_m$ [54,64,67,82]. The transversal coupling strength $J/\gamma = 35$, the decay rate $\kappa/\gamma = 1$, and the relative phase $\theta = 0$, where $\gamma/2\pi = 1$ MHz is used as an energy unit throughout the paper.

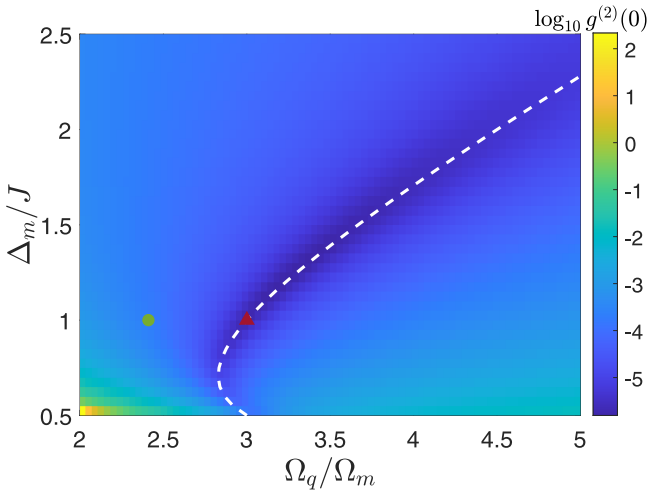

FIG. 3. Logarithm function of the equal-time second-order correlation function $\log_{10} g^{(2)}(0)$ in the space of the ratios Δ_m/J and Ω_q/Ω_m. The white dashed line follows the optimal ratio Ω_q/Ω_m in Eq. (16). The red triangle distinguishes the resonant case with $\Delta_q = \Delta_m$ [54,67,82] and the green circle marks the less optimized results obtained in Refs. [55,64]. Δ_q is set by the optimized condition in Eq. (15) and the other parameters are set the same as Fig. 2.

$\mathcal{L}_o[\rho] = 2o\rho o^\dagger - o^\dagger o\rho - \rho o^\dagger o$ [85], with $o = m, \sigma_-$ indicating, respectively, the decay channels for the magnon mode and the qubit. In our simulation, the Hilbert space is truncated up to a limited number of Fock state $|N\rangle$ with $N = 10$. The decay rates of the magnon and qubit are set as $\kappa_m = \kappa_q = \kappa$ for simplicity.

Figure 2 is devoted to confirming Eq. (15), for which we employ the optimized condition in Eq. (16) and set $\theta = 0$ for simplicity. In the space of Δ_q/J and Δ_m/J, it is interesting to find that the single-magnon occupation P_1 is always maximized with the optimized condition $\Delta_q\Delta_m \approx J^2$ in Eq. (15), which is marked by the black dashed line. For example, we have $P_1 \sim 0.11$ when $\Delta_m/J = 3/4$ and $\Delta_q/J = 4/3$. In addition, the optimal condition [54,64,67,82] found for the resonant case is confirmed and marked by the red triangle.

In Fig. 3, we plot the $g^{(2)}$ function to check Eq. (16) with respect to the ratios Δ_m/J and Ω_q/Ω_m. It is found that the optimized point Ω_q/Ω_m for the minimization of $g^{(2)}(0)$ varies with Δ_m/J. In particular, the $g^{(2)}$ function is minimized to be $g^{(2)}(0) \sim 10^{-5.3}$ when $\Omega_q/\Omega_m = 2.85$ and $\Delta_m/J = 0.8$, $g^{(2)}(0) \sim 10^{-5.7}$ when $\Omega_q/\Omega_m = 3$ and $\Delta_m/J = 1$, $g^{(2)}(0) \sim 10^{-5.8}$ when $\Omega_q/\Omega_m = 3.23$ and $\Delta_m/J = 1.2$, and $g^{(2)}(0) \sim 10^{-5.4}$ when $\Omega_q/\Omega_m = 4.5$ and $\Delta_m/J = 2$. It is straightforward to verify that these optimized ratios Ω_q/Ω_m are exactly the same as the analytical result in Eq. (16), which is marked by the white dashed line. Around the red triangle, our analytical expression in Eq. (16) under the resonant condition confirms the optimal ratio $\Omega_q/\Omega_m = 3$ for the blockade numerically obtained in Refs. [54,67,82], which is more accurate than that (see the green circle) analytically obtained in Refs. [55,64] on an inaccurate assumption $C_{g2} = 0$.

Following Eqs. (15) and (16), the optimized condition (18) about the relative phase θ between the probing and driving fields is confirmed in Fig. 4. It is found that the $g^{(2)}$ function of the stable single-magnon state can be further reduced by an optimal relative phase. In particular, when the driving and probing fields are in phase, i.e., $\theta = 0$, the $g^{(2)}$ function is about $g^{(2)}(0) \sim 10^{-5.3}$ for $\Delta_m/J = 0.8$, $g^{(2)}(0) \sim 10^{-5.7}$ for $\Delta_m/J = 1$, and $g^{(2)}(0) \sim 10^{-5.8}$ for $\Delta_m/J = 1.2$. In contrast, the purity of the single-magnon state can be further enhanced to $g^{(2)}(0) \sim 10^{-6.0}$ by $\theta/\pi = 0.7 \times 10^{-2}$ for $\Delta_m/J = 0.8$, by $\theta/\pi = 0.6 \times 10^{-2}$ for $\Delta_m/J = 1$, and by $\theta/\pi = 0.5 \times 10^{-2}$

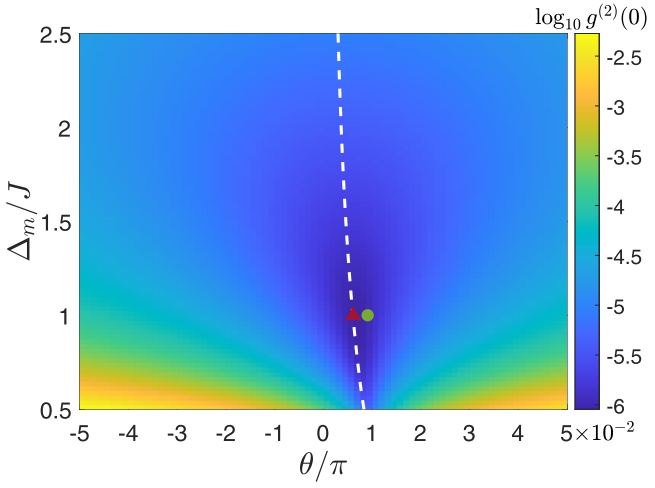

FIG. 4. Logarithmic function of the equal-time second-order correlation function $\log_{10} g^{(2)}(0)$ vs the relative phase θ and the ratio Δ_m/J. The white dashed line follows the optimal phase θ_{opt} given in Eq. (18). The red triangle and the green circle describes our result and the existing one [55,64] for the resonant case $\Delta_m = \Delta_q$, respectively. Δ_q and Ω_q are set by the optimized conditions in Eq. (15) and (16), respectively. The other parameters are set the same as Fig. 2.

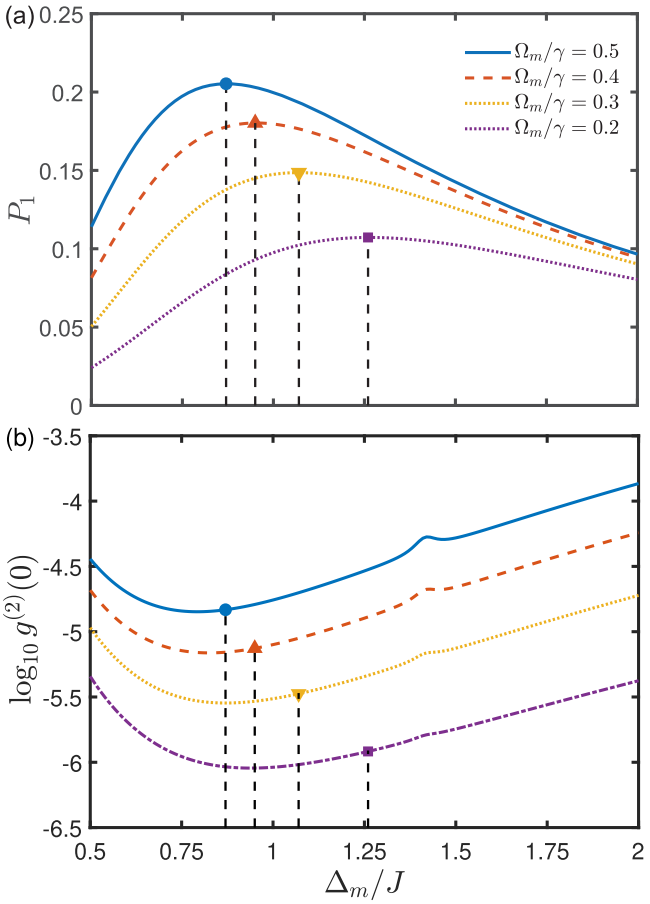

FIG. 5. (a) Single-magnon probability P_1 and (b) logarithmic function of the equal-time second-order correlation function $\log_{10} g^{(2)}(0)$ vs the ratio Δ_m/J under various driving intensities Ω_m/γ. Δ_q, Ω_q, and θ are set by the optimized conditions in Eqs. (15), (16), and (18), respectively. The other parameters are set as $J/\gamma = 35$ and $\kappa/\gamma = 1$.

for $\Delta_m/J = 1.2$. All these nonvanishing phases can be analytically obtained by $\theta_{\rm opt}$ in Eq. (18), which are marked by the white dashed line. The red triangle and the green circle denote our result and the previous optimized result [55,64], respectively, for the resonant case.

C. Approach high-quality single-magnon state

Running the master equation (19) with all the optimal conditions in Eqs. (15), (16), and (18), we are now on the stage approaching a steady and high-quality single-magnon state though parametric optimization over P_1 and $g^{(2)}(0)$.

In Fig. 5 under various driving intensities Ω_m/γ, we demonstrate P_1 and the $g^{(2)}$ function of the stabilized single-magnon state with respect to the ratio Δ_m/J. Under the constraints of Eqs. (15), (16), and (18), we are left with three tunable parameters Δ_m, J, and κ in determining these statistical properties. It is found that a stronger driving intensity Ω_m/γ gives rise to a larger P_1 yet accompanied with a larger $g^{(2)}(0)$. In particular, when $\Delta_m/J = 1$, i.e., the magnon and qubit are resonant due to $\Delta_q\Delta_m = J^2$, the single-magnon occupation P_1 ranges from 0.09 to 0.20 and correspondingly, the

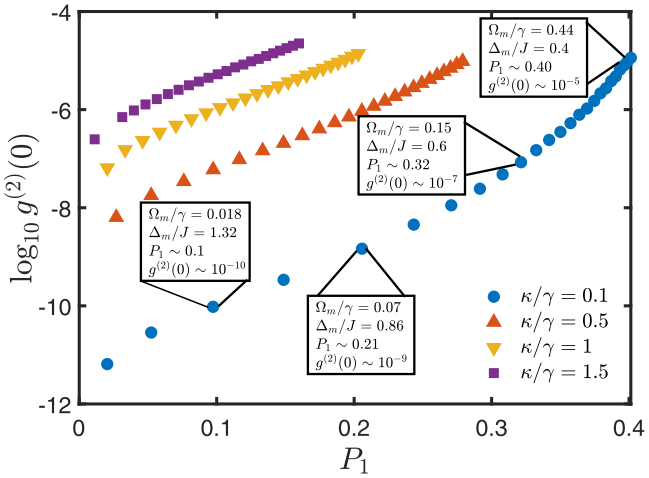

FIG. 6. Logarithmic function of the equal-time second-order correlation function $\log_{10} g^{(2)}(0)$ vs the single-excitation probability P_1 for various decay rates κ and driving intensity $\Omega_m/\gamma \in (0.005, 0.5)$. Each point is obtained with optimized detuning Δ_m/J. The other parameters are set the same as Fig. 5.

equal-time second-order correlation function $g^{(2)}(0)$ is in the range of $(10^{-6.0}, 10^{-4.8})$ for $\Omega_m/\gamma \in (0.2, 0.5)$. All of these results could be further optimized by tuning the magnon-qubit detuning, i.e., $\Delta_m/J \neq 1$. For $\Omega_m/\gamma = 0.2$, P_1 is maximized to be $P_1 \sim 0.11$ and $g^{(2)}(0) \sim 10^{-5.9}$ when $\Delta_m/J = 1.26$; for $\Omega_m/\gamma = 0.3$, $P_1 \sim 0.15$ and $g^{(2)}(0) \sim 10^{-5.5}$ when $\Delta_m/J = 1.07$; for $\Omega_m/\gamma = 0.4$, $P_1 \sim 0.18$ and $g^{(2)}(0) \sim 10^{-5.1}$ when $\Delta_m/J = 0.95$; and for $\Omega_m/\gamma = 0.5$, $P_1 \sim 0.20$ and $g^{(2)}(0) \sim 10^{-4.8}$ when $\Delta_m/J = 0.87$. In each curve of Figs. 5(a) and 5(b) with the same driving intensity, one can locate a maximal P_1 or a minimal $g^{(2)}(0)$. The optimized points do not always share the same detuning Δ_m, which implies that a compromise has to be made to balance the two indicators.

Due to the probability amplitude C_{g1} in Eq. (12a) that is under the constraint of Eq. (15), P_1 can be further enhanced by decreasing the decay rate κ. In Fig. 6, we demonstrate the $g^{(2)}$ function versus P_1 with optimized Δ_m/J for various driving intensities and decay rates. Each point is obtained by locating the optimized Δ_m/J in a similar way as that in Fig. 5(a). One can see that $\log_{10} g^{(2)}(0)$ and P_1 manifest an almost linear relationship for various κ when Ω_m/γ runs from 0.005 to 0.5. More important, it is found that when the decay rate is as low as $\kappa/\gamma = 0.1$, a single-magnon state presents with a large brightness and a high degree of purity, e.g., $P_1 \sim 0.21$ and $g^{(2)}(0) \sim 10^{-9}$ when $\Omega_m/\gamma = 0.07$ and $\Delta_m/J = 0.86$; $P_1 \sim 0.32$ and $g^{(2)}(0) \sim 10^{-7.0}$ when $\Omega_m/\gamma = 0.15$ and $\Delta_m/J = 0.6$; and $P_1 \sim 0.40$ and $g^{(2)}(0) \sim 10^{-5.0}$ when $\Omega_m/\gamma = 0.44$ and $\Delta_m/J = 0.4$.

All these results prevail over the existing ones in a similar scenario. In the quantum dot-cavity system, the single-photon state with $P_1 \sim 0.06$ and $g^{(2)}(0) \sim 10^{-2}$ has been proposed in theory [64]; and that with $P_1 \sim 0.01$ and $g^{(2)}(0) \sim 10^{-2}$ [69] can be experimentally demonstrated. In a cavity QED system [66], the single-photon state can achieve $P_1 \sim 0.08$ and $g^{(2)}(0) \sim 10^{-1.5}$ by using the optical Stark shift, and can achieve $P_1 \sim 0.01$ and $g^{(2)}(0) \sim 10^{-5}$ in a double-cavity system with ultrastrong optomechanical coupling. Using the

TABLE I. Comparison of our proposal and the existing ones for a stable single-quantum state.

Proposals/systems	Experiment/theory	P_1	$g^{(2)}(0)$	ρ_{steady}
Our work	Theory	~ 0.40	$\sim 10^{-5}$	$\approx 0.6\|0\rangle\langle 0\| + 0.4\|1\rangle\langle 1\| + 10^{-6}\|2\rangle\langle 2\|$
Quantum dot cavity QED system [69]	Experiment	~ 0.01	$\sim 10^{-2}$	$\approx 0.99\|0\rangle\langle 0\| + 0.01\|1\rangle\langle 1\| + 10^{-6}\|2\rangle\langle 2\|$
Cavity QED system [66]	Theory	~ 0.08	$\sim 10^{-1.5}$	$\approx 0.92\|0\rangle\langle 0\| + 0.08\|1\rangle\langle 1\| + 10^{-5}\|2\rangle\langle 2\|$
Photonic crystal cavity system[a] [71]	Theory	~ 0.10	$\sim 10^{-2}$	$\approx 0.90\|0\rangle\langle 0\| + 0.10\|1\rangle\langle 1\| + 10^{-4}\|2\rangle\langle 2\|$
Double-cavity system[b] [70]	Theory	~ 0.01	$\sim 10^{-5}$	$\approx 0.99\|0\rangle\langle 0\| + 0.01\|1\rangle\langle 1\| + 10^{-9}\|2\rangle\langle 2\|$
Hybrid magnonic system[c] [55]	Theory	~ 0.05	$\sim 10^{-2}$	$\approx 0.95\|0\rangle\langle 0\| + 0.05\|1\rangle\langle 1\| + 10^{-4}\|2\rangle\langle 2\|$

[a]Photonic crystal cavity system via two-photon absorption process of the environment.
[b]Double-cavity system relying on the ultrastrong optomechanical interaction, which is actually challenging for the state-of-art experiment [70].
[c]Hybrid magnonic system in which the magnon is coupled to the qubit mediated by a microwave cavity.

two-photon absorption process of environment [71], the brightness of the single-photon state can be improved to $P_1 \sim 0.1$ at the cost of a suppressed purity of $g^{(2)}(0) \sim 10^{-2}$. In a hybrid system established by the indirect interaction between magnon and qubit mediated by a microwave cavity [55], the single-magnon state is found to end up with $P_1 \sim 0.05$ and $g^{(2)}(0) \sim 10^{-2}$ when the second-excitation probability is improperly omitted in the calculation of the optimized conditions. In Table I, we list some representative results for P_1, $g^{(2)}(0)$, and the steady-state density matrix ρ_{steady} of the interested mode.

IV. GENERAL SITUATION IN THE PRESENCE OF N MAGNONS

Our proposal can be extended to consider the statistical properties of any one of the N magnon modes of the same frequency ω_m that are uniformly coupled to a common qubit with the coupling strength J. In this general situation, the preceding optimized conditions for the ratio of the probing intensity to the driving intensity Ω_q/Ω_m and the relative phase between the two fields θ are scale free and only that for the detunings $\Delta_q\Delta_m/J^2$ in Eq. (15) is modified to scale with N. The total Hamiltonian (2) including the probing field on qubit and the driving fields on magnons is now rewritten as

$$H_{\text{tot}} = \left[\Omega_m \sum_{j=1}^{N} m_j^\dagger e^{-i\omega t} + \Omega_q \sigma_+ e^{-i(\omega t+\theta)} + \text{H.c.}\right] + \omega_q \sigma_+\sigma_- + \omega_m \sum_{j=1}^{N} m_j^\dagger m_j + J\sum_{j=1}^{N}(m_j\sigma_+ + m_j^\dagger\sigma_-), \tag{20}$$

where $m_j^\dagger$ and m_j are the creation and annihilation operators of the jth magnon mode and θ remains as the relative phase of the fields. Then, in the rotating frame with respect to $H' = \omega(\sum_{j=1}^{N} m_j^\dagger m_j + \sigma_+\sigma_-)$, the effective Hamiltonian becomes

$$H_{\text{eff}} = \Omega_m \sum_{j=1}^{N}(m_j^\dagger + m_j) + \Omega_q(\sigma_+ e^{-i\theta} + \sigma_- e^{i\theta}) + \Delta_q\sigma_+\sigma_- + \Delta_m \sum_{j=1}^{N} m_j^\dagger m_j + J\sum_{j=1}^{N}(m_j\sigma_+ + m_j^\dagger\sigma_-). \tag{21}$$

Following the analytical model [54–57,63–66], the non-Hermitian Hamiltonian in Eq. (9) and the approximated system state in Eq. (10) in the low-excitation subspace are modified to be

$$H_{\text{non}} = H_{\text{eff}} - i\frac{\kappa}{2}\left(\sigma_+\sigma_- + \sum_{j=1}^{N} m_j^\dagger m_j\right), \quad |\psi\rangle = |\psi_0\rangle + |\psi_1\rangle + |\psi_2\rangle, \tag{22}$$

respectively. Here, H_{eff} is the effective Hamiltonian in Eq. (21) and the subscript in $|\psi_k\rangle$, $k = 0, 1, 2$, implies the state with k excitations. In particular, we have

$$\begin{aligned} |\psi_0\rangle &= C_{g_0}|g\rangle|0\rangle^{\otimes N}, \\ |\psi_1\rangle &= C_{e_0}|e\rangle|0\rangle^{\otimes N} + \sum_{j=1}^{N} C_{g_j} m_j^\dagger|g\rangle|0\rangle^{\otimes N}, \\ |\psi_2\rangle &= \sum_{j=1}^{N} C_{e_j} m_j^\dagger|e\rangle|0\rangle^{\otimes N} + \sum_{j,k=1}^{N} C_{g_{jk}} m_j^\dagger m_k^\dagger|g\rangle|0\rangle^{\otimes N}, \end{aligned} \tag{23}$$

where $m_j^\dagger|0\rangle^{\otimes N}$ describes that the jth magnon is excited and C_α ($\alpha = g_0, e_0, g_j, e_j, g_{jk}$) is the probability amplitude for the relevant base. Due to the system symmetry, one can focus on the first magnon by assuming that the bases of the same number of excitations share the same amplitude, i.e., $C_{g_1} = C_{g_j}$, $2 \leqslant j \leqslant N$, and $C_{g_{12}} = C_{g_{1j}}$, $2 < j \leqslant N$. Then, the steady-state amplitudes are

$$\begin{aligned} C_{g_1} &= \frac{J\Omega_q e^{-i\theta} - \Omega_m\tilde{\Delta}_q}{\tilde{\Delta}_q\tilde{\Delta}_m - NJ^2}, \\ C_{g_{11}} &\approx \frac{\sqrt{2}(AC_{g_1} - B)}{2\tilde{\Delta}_m(\tilde{\Delta}_q + \tilde{\Delta}_m) - 2J^2}, \\ C_{e_1} &\approx \frac{-(\Omega_q e^{-i\theta}\tilde{\Delta}_q - NJ\Omega_m)C_{g_1}}{\tilde{\Delta}_q(\tilde{\Delta}_q + \tilde{\Delta}_m)} + \frac{B}{J(\tilde{\Delta}_q + \tilde{\Delta}_m)}, \end{aligned} \tag{24}$$

where the coefficient A becomes N-dependent

$$A = J\Omega_q e^{-i\theta} - \left[(\tilde{\Delta}_q + \tilde{\Delta}_m) + \frac{NJ^2}{\tilde{\Delta}_q}\right]\Omega_m, \tag{25}$$

which is consistent with Eq. (13), and B remains invariant. Subsequently, it is found that the optimized condition for maximizing P_1 in Eq. (15) scales with the system size N,

$$\Delta_q\Delta_m \approx \tilde{\Delta}_q\tilde{\Delta}_m = NJ^2, \tag{26}$$

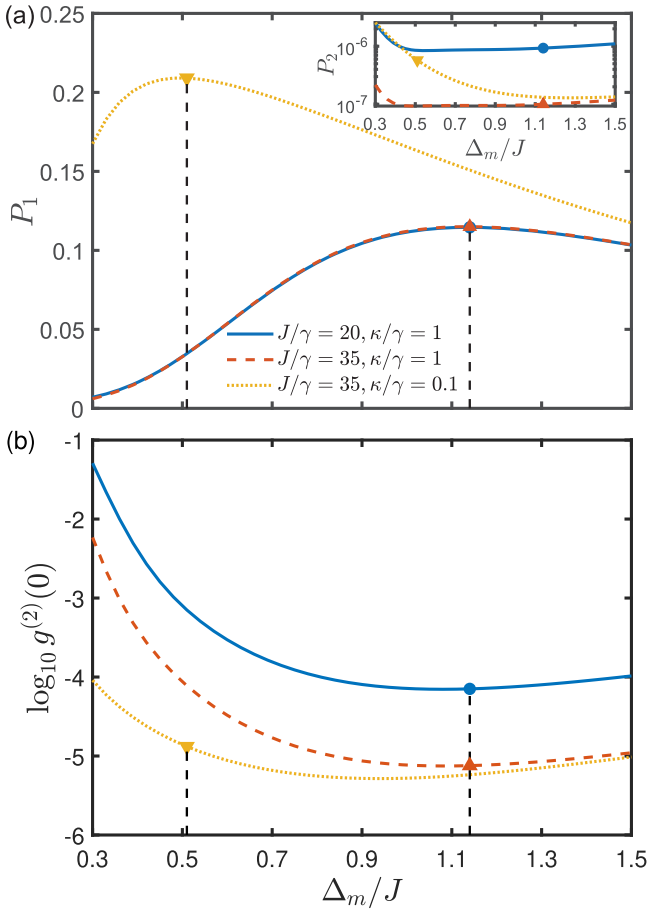

FIG. 7. (a) Single-magnon probability P_1 and (b) Logarithmic function of the equal-time second-order correlation function $\log_{10} g^{(2)}(0)$ vs the ratio Δ_m/J under various coupling strengths J/γ and decay rates κ/γ. Inset: Double-magnon probability P_2 vs Δ_m/J. Δ_q, Ω_q, and θ are set according to the optimized conditions in Eqs. (26), (16), and (18), respectively. The driving intensity is fixed as $\Omega_m/\gamma = 0.44$.

and the other two conditions about Ω_q/Ω_m in Eq. (16) and θ in Eq. (18) are found to be scale free.

To numerically simulate the single-magnon state in a double-magnon system, we use the effective Hamiltonian H_{eff} in Eq. (21) and the master equation (19) with the addition of the decay channel for the second magnon mode. In Figs. 7(a) and 7(b) for various coupling strengths J/γ and decay rates κ/γ, we demonstrate the single-magnon probability P_1 and the $g^{(2)}$ function for the first magnon mode with respect to the ratio Δ_m/J. It is found that roughly a stronger J/γ and a weaker κ/γ yield a larger P_1 and a smaller $g^{(2)}(0)$ for any Δ_m/J. In Fig. 7, although P_1 is not sensitive to the coupling strength in the presence of a weak decay rate, P_2 as well as $g^{(2)}(0)$ can be much suppressed by a strong J/γ. In particular, when $\kappa/\gamma = 1$, P_1 is optimized as $P_1 \sim 0.12$ with $\Delta_m/J = 1.15$ for both $J/\gamma = 20$ and $J/\gamma = 35$. In the former case, $P_2 \sim 10^{-6}$ and $g^{(2)}(0) \sim 10^{-4.1}$, while in the latter case, $P_2 \sim 10^{-7}$ and $g^{(2)}(0) \sim 10^{-5.1}$. When the decay rate is as low as $\kappa/\gamma = 0.1$, P_1 is optimized to be $P_1 \sim 0.21$ by $\Delta_m/J = 0.51$ and $J/\gamma = 35$, which is accompanied by $P_2 \sim 10^{-6}$ and $g^{(2)}(0) \sim 10^{-5.0}$.

V. CONCLUSION

In summary, we present a systematic optimization process to analytically obtain the optimal conditions for the strong magnon blockade, which produces in a long-time limit a high-quality (a large brightness and a high purity) single-magnon state in a hybrid magnon-qubit system by exploiting the strong coupling strength between two components, their weak decay rates, their frequency detunings Δ_q and Δ_m, the intensity ratio of driving and probing fields Ω_q/Ω_m, and their relative phase θ. Through parametric optimization, we confirm that under the optimized conditions, i.e., Eqs. (15) or (26) for $\Delta_q\Delta_m$, Eq. (16) for Ω_q/Ω_m, and Eq. (18) for θ, the single-magnon probability P_1 and the equal-time second-order correlation function $g^{(2)}(0)$ could be compromisingly amplified and suppressed, respectively. It is interesting to find that with strong driving intensity and weak decay rates, a single-magnon state with a large brightness and a high purity, i.e., $P_1 \sim 0.40$ and $g^{(2)}(0) \sim 10^{-5}$, can be prepared in a qubit-magnon system. The optimized conditions presented in our proposal, scaling with the system size or scale free, are actually system independent. Our study thus paves a way toward stabilizing a high-quality single-quantum source for the quantum information process based on a macroscopic spin system, and it is extendable to other bosonic systems.

ACKNOWLEDGMENT

We acknowledge grant support from the National Natural Science Foundation of China (Grant No. 11974311).

[1] A. Serga, A. V. Chumak, and B. Hillebrands, YIG magnonics, J. Phys. D: Appl. Phys. **43**, 264002 (2010).
[2] A. V. Chumak, V. Vasyuchka, A. Serga, and B. Hillebrands, Magnon spintronics, Nat. Phys. **11**, 453 (2015).
[3] S. Zheng, Z. Wang, Y. Wang, F. Sun, Q. He, P. Yan, and H. Y. Yuan, Tutorial: Nonlinear magnonics, J. Appl. Phys. **134**, 151101 (2023).
[4] M. Wallquist, K. Hammerer, P. Rabl, M. Lukin, and P. Zoller, Hybrid quantum devices and quantum engineering, Phys. Scr. **T137**, 014001 (2009).
[5] H. J. Kimble, The quantum internet, Nature (London) **453**, 1023 (2008).
[6] G. Kurizki, P. Bertet, Y. Kubo, K. Mølmer, D. Petrosyan, P. Rabl, and J. Schmiedmayer, Quantum technologies with hybrid systems, Proc. Natl. Acad. Sci. USA **112**, 3866 (2015).
[7] O. O. Soykal and M. E. Flatté, Strong field interactions between a nanomagnet and a photonic cavity, Phys. Rev. Lett. **104**, 077202 (2010).
[8] H. Huebl, C. W. Zollitsch, J. Lotze, F. Hocke, M. Greifenstein, A. Marx, R. Gross, and S. T. B. Goennenwein, High

cooperativity in coupled microwave resonator ferrimagnetic insulator hybrids, Phys. Rev. Lett. **111**, 127003 (2013).

[9] X. Zhang, C.-L. Zou, L. Jiang, and H. X. Tang, Strongly coupled magnons and cavity microwave photons, Phys. Rev. Lett. **113**, 156401 (2014).

[10] Y. Tabuchi, S. Ishino, T. Ishikawa, R. Yamazaki, K. Usami, and Y. Nakamura, Hybridizing ferromagnetic magnons and microwave photons in the quantum limit, Phys. Rev. Lett. **113**, 083603 (2014).

[11] X. Zhang, C.-L. Zou, L. Jiang, and H. X. Tang, Cavity magnomechanics, Sci. Adv. **2**, e1501286 (2016).

[12] J. Li, S.-Y. Zhu, and G. S. Agarwal, Magnon-photon-phonon entanglement in cavity magnomechanics, Phys. Rev. Lett. **121**, 203601 (2018).

[13] Z. Shen, G.-T. Xu, M. Zhang, Y.-L. Zhang, Y. Wang, C.-Z. Chai, C.-L. Zou, G.-C. Guo, and C.-H. Dong, Coherent coupling between phonons, magnons, and photons, Phys. Rev. Lett. **129**, 243601 (2022).

[14] M. Goryachev, W. G. Farr, D. L. Creedon, Y. Fan, M. Kostylev, and M. E. Tobar, High-cooperativity cavity QED with magnons at microwave frequencies, Phys. Rev. Appl. **2**, 054002 (2014).

[15] M. Mergenthaler, J. Liu, J. J. Le Roy, N. Ares, A. L. Thompson, L. Bogani, F. Luis, S. J. Blundell, T. Lancaster, A. Ardavan, G. A. D. Briggs, P. J. Leek, and E. A. Laird, Strong coupling of microwave photons to antiferromagnetic fluctuations in an organic magnet, Phys. Rev. Lett. **119**, 147701 (2017).

[16] J. Bourhill, N. Kostylev, M. Goryachev, D. L. Creedon, and M. E. Tobar, Ultrahigh cooperativity interactions between magnons and resonant photons in a YIG sphere, Phys. Rev. B **93**, 144420 (2016).

[17] N. Kostylev, M. Goryachev, and M. E. Tobar, Superstrong coupling of a microwave cavity to yttrium iron garnet magnons, Appl. Phys. Lett. **108**, 062402 (2016).

[18] A. Osada, R. Hisatomi, A. Noguchi, Y. Tabuchi, R. Yamazaki, K. Usami, M. Sadgrove, R. Yalla, M. Nomura, and Y. Nakamura, Cavity optomagnonics with spin-orbit coupled photons, Phys. Rev. Lett. **116**, 223601 (2016).

[19] X. Zhang, N. Zhu, C.-L. Zou, and H. X. Tang, Optomagnonic whispering gallery microresonators, Phys. Rev. Lett. **117**, 123605 (2016).

[20] J. A. Haigh, A. Nunnenkamp, A. J. Ramsay, and A. J. Ferguson, Triple-resonant Brillouin light scattering in magneto-optical cavities, Phys. Rev. Lett. **117**, 133602 (2016).

[21] A. Osada, A. Gloppe, R. Hisatomi, A. Noguchi, R. Yamazaki, M. Nomura, Y. Nakamura, and K. Usami, Brillouin light scattering by magnetic quasivortices in cavity optomagnonics, Phys. Rev. Lett. **120**, 133602 (2018).

[22] T. S. Parvini, V. A. S. V. Bittencourt, and S. V. Kusminskiy, Antiferromagnetic cavity optomagnonics, Phys. Rev. Res. **2**, 022027 (2020).

[23] Y. Tabuchi, S. Ishino, A. Noguchi, T. Ishikawa, R. Yamazaki, K. Usami, and Y. Nakamura, Coherent coupling between a ferromagnetic magnon and a superconducting qubit, Science **349**, 405 (2015).

[24] D. Lachance-Quirion, Y. Tabuchi, S. Ishino, A. Noguchi, T. Ishikawa, R. Yamazaki, and Y. Nakamura, Resolving quanta of collective spin excitations in a millimeter-sized ferromagnet, Sci. Adv. **3**, e1603150 (2017).

[25] D. Lachance-Quirion, S. P. Wolski, Y. Tabuchi, S. Kono, K. Usami, and Y. Nakamura, Entanglement-based single-shot detection of a single magnon with a superconducting qubit, Science **367**, 425 (2020).

[26] D. Xu, X.-K. Gu, H.-K. Li, Y.-C. Weng, Y.-P. Wang, J. Li, H. Wang, S.-Y. Zhu, and J. Q. You, Quantum control of a single magnon in a macroscopic spin system, Phys. Rev. Lett. **130**, 193603 (2023).

[27] S. P. Wolski, D. Lachance-Quirion, Y. Tabuchi, S. Kono, A. Noguchi, K. Usami, and Y. Nakamura, Dissipation-based quantum sensing of magnons with a superconducting qubit, Phys. Rev. Lett. **125**, 117701 (2020).

[28] M. Kounalakis, G. E. W. Bauer, and Y. M. Blanter, Analog quantum control of magnonic cat states on a chip by a superconducting qubit, Phys. Rev. Lett. **129**, 037205 (2022).

[29] A. Imamoğlu, Cavity QED based on collective magnetic dipole coupling: Spin ensembles as hybrid two-level systems, Phys. Rev. Lett. **102**, 083602 (2009).

[30] Y.-P. Wang, G.-Q. Zhang, D. Zhang, T.-F. Li, C.-M. Hu, and J. Q. You, Bistability of cavity magnon polaritons, Phys. Rev. Lett. **120**, 057202 (2018).

[31] G.-Q. Zhang, Y.-P. Wang, and J. Q. You, Theory of the magnon Kerr effect in cavity magnonics, Sci. China Phys. Mech. Astron. **62**, 987511 (2019).

[32] R.-C. Shen, Y.-P. Wang, J. Li, S.-Y. Zhu, G. S. Agarwal, and J. Q. You, Long-time memory and ternary logic gate using a multistable cavity magnonic system, Phys. Rev. Lett. **127**, 183202 (2021).

[33] Z. Wang, H. Y. Yuan, Y. Cao, Z.-X. Li, R. A. Duine, and P. Yan, Magnonic frequency comb through nonlinear magnon-skyrmion scattering, Phys. Rev. Lett. **127**, 037202 (2021).

[34] J. W. Rao, B. Yao, C. Y. Wang, C. Zhang, T. Yu, and W. Lu, Unveiling a pump-induced magnon mode via its strong interaction with Walker modes, Phys. Rev. Lett. **130**, 046705 (2023).

[35] Z. Wang, H. Y. Yuan, Y. Cao, and P. Yan, Twisted magnon frequency comb and Penrose superradiance, Phys. Rev. Lett. **129**, 107203 (2022).

[36] M. Amazioug, B. Teklu, and M. Asjad, Enhancement of magnon-photon-phonon entanglement in a cavity magnomechanics with coherent feedback loop, Sci. Rep. **13**, 3833 (2023).

[37] H. Y. Yuan, P. Yan, S. Zheng, Q. Y. He, K. Xia, and M.-H. Yung, Steady Bell state generation via magnon-photon coupling, Phys. Rev. Lett. **124**, 053602 (2020).

[38] S.-F. Qi and J. Jing, Generation of Bell and Greenberger-Horne-Zeilinger states from a hybrid qubit-photon-magnon system, Phys. Rev. A **105**, 022624 (2022).

[39] H. Y. Yuan, S. Zheng, Z. Ficek, Q. Y. He, and M.-H. Yung, Enhancement of magnon-magnon entanglement inside a cavity, Phys. Rev. B **101**, 014419 (2020).

[40] V. A. Mousolou, Y. Liu, A. Bergman, A. Delin, O. Eriksson, M. Pereiro, D. Thonig, and E. Sjöqvist, Magnon-magnon entanglement and its quantification via a microwave cavity, Phys. Rev. B **104**, 224302 (2021).

[41] Y.-L. Ren, J.-K. Xie, X.-K. Li, S.-L. Ma, and F.-L. Li, Long-range generation of a magnon-magnon entangled state, Phys. Rev. B **105**, 094422 (2022).

[42] R. Hisatomi, A. Osada, Y. Tabuchi, T. Ishikawa, A. Noguchi, R. Yamazaki, K. Usami, and Y. Nakamura, Bidirectional conversion between microwave and light via ferromagnetic magnons, Phys. Rev. B **93**, 174427 (2016).

[43] N. Zhu, X. Zhang, X. Han, C.-L. Zou, C. Zhong, C.-H. Wang, L. Jiang, and H. X. Tang, Waveguide cavity optomagnonics for microwave-to-optics conversion, Optica **7**, 1291 (2020).

[44] Q. Cai, J. Liao, B. Shen, G. Guo, and Q. Zhou, Microwave quantum illumination via cavity magnonics, Phys. Rev. A **103**, 052419 (2021).

[45] G.-Q. Zhang, Y. Wang, and W. Xiong, Detection sensitivity enhancement of magnon Kerr nonlinearity in cavity magnonics induced by coherent perfect absorption, Phys. Rev. B **107**, 064417 (2023).

[46] M. Hofheinz, E. M. Weig, M. Ansmann, R. C. Bialczak, E. Lucero, M. Neeley, A. D. O'Connell, H. Wang, J. M. Martinis, and A. N. Cleland, Generation of Fock states in a superconducting quantum circuit, Nature (London) **454**, 310 (2008).

[47] A. D. O'Connell, M. Hofheinz, M. Ansmann, R. C. Bialczak, M. Lenander, E. Lucero, M. Neeley, D. Sank, H. Wang, M. Weides, J. Wenner, J. M. Martinis, and A. N. Cleland, Quantum ground state and single-phonon control of a mechanical resonator, Nature (London) **464**, 697 (2010).

[48] S. Hong, R. Riedinger, I. Marinković, A. Wallucks, S. G. Hofer, R. A. Norte, M. Aspelmeyer, and S. Gröblacher, Hanbury Brown and Twiss interferometry of single phonons from an optomechanical resonator, Science **358**, 203 (2017).

[49] Y. Chu, P. Kharel, T. Yoon, L. Frunzio, P. T. Rakich, and R. J. Schoelkopf, Creation and control of multi-phonon Fock states in a bulk acoustic-wave resonator, Nature (London) **563**, 666 (2018).

[50] V. A. S. V. Bittencourt, V. Feulner, and S. V. Kusminskiy, Magnon heralding in cavity optomagnonics, Phys. Rev. A **100**, 013810 (2019).

[51] F.-X. Sun, S.-S. Zheng, Y. Xiao, Q. Gong, Q. He, and K. Xia, Remote generation of magnon Schrödinger cat state via magnon-photon entanglement, Phys. Rev. Lett. **127**, 087203 (2021).

[52] S. Sharma, V. S. V. Bittencourt, and S. V. Kusminskiy, Protocol for generating an arbitrary quantum state of the magnetization in cavity magnonics, J. Phys. Mater. **5**, 034006 (2022).

[53] S. He, X. Xin, F.-Y. Zhang, and C. Li, Generation of a Schrödinger cat state in a hybrid ferromagnet-superconductor system, Phys. Rev. A **107**, 023709 (2023).

[54] Z.-X. Liu, H. Xiong, and Y. Wu, Magnon blockade in a hybrid ferromagnet-superconductor quantum system, Phys. Rev. B **100**, 134421 (2019).

[55] J.-K. Xie, S.-L. Ma, and F.-L. Li, Quantum-interference-enhanced magnon blockade in an yttrium-iron-garnet sphere coupled to superconducting circuits, Phys. Rev. A **101**, 042331 (2020).

[56] K. Wu, W.-X. Zhong, G.-L. Cheng, and A.-X. Chen, Phase-controlled multimagnon blockade and magnon-induced tunneling in a hybrid superconducting system, Phys. Rev. A **103**, 052411 (2021).

[57] F. Wang, C. Gou, J. Xu, and C. Gong, Hybrid magnon-atom entanglement and magnon blockade via quantum interference, Phys. Rev. A **106**, 013705 (2022).

[58] H. Y. Yuan and R. A. Duine, Magnon antibunching in a nanomagnet, Phys. Rev. B **102**, 100402 (2020).

[59] B. Lounis and M. Orrit, Single-photon sources, Rep. Prog. Phys. **68**, 1129 (2005).

[60] M. D. Eisaman, J. Fan, A. Migdall, and S. V. Polyakov, Invited review article: Single-photon sources and detectors, Rev. Sci. Instrum. **82**, 071101 (2011).

[61] P. Rabl, Photon blockade effect in optomechanical systems, Phys. Rev. Lett. **107**, 063601 (2011).

[62] G. J. Milburn and S. Basiri-Esfahani, Quantum optics with one or two photons, Proc. R. Soc. A. **471**, 20150208 (2015).

[63] P. Kómár, S. D. Bennett, K. Stannigel, S. J. M. Habraken, P. Rabl, P. Zoller, and M. D. Lukin, Single-photon nonlinearities in two-mode optomechanics, Phys. Rev. A **87**, 013839 (2013).

[64] J. Tang, W. Geng, and X. Xu, Quantum interference induced photon blockade in a coupled single quantum dot-cavity system, Sci. Rep. **5**, 9252 (2015).

[65] H. Flayac and V. Savona, Unconventional photon blockade, Phys. Rev. A **96**, 053810 (2017).

[66] J. Tang, Y. Deng, and C. Lee, Strong photon blockade mediated by optical Stark shift in a single-atom-cavity system, Phys. Rev. Appl. **12**, 044065 (2019).

[67] Z. Li, X. Li, and X. Zhong, Strong photon blockade in an all-fiber emitter-cavity quantum electrodynamics system, Phys. Rev. A **103**, 043724 (2021).

[68] C. Couteau, S. Barz, T. Durt, T. Gerrits, J. Huwer, R. Prevedel, J. Rarity, A. Shields, and G. Weihs, Applications of single photons to quantum communication and computing, Nat. Rev. Phys. **5**, 326 (2023).

[69] H. J. Snijders, J. A. Frey, J. Norman, H. Flayac, V. Savona, A. C. Gossard, J. E. Bowers, M. P. van Exter, D. Bouwmeester, and W. Löffler, Observation of the unconventional photon blockade, Phys. Rev. Lett. **121**, 043601 (2018).

[70] D.-Y. Wang, C.-H. Bai, S. Liu, S. Zhang, and H.-F. Wang, Photon blockade in a double-cavity optomechanical system with nonreciprocal coupling, New J. Phys. **22**, 093006 (2020).

[71] Y.-H. Zhou, X.-Y. Zhang, T. Liu, Q.-C. Wu, Z.-C. Shi, H.-Z. Shen, and C.-P. Yang, Environmentally induced photon blockade via two-photon absorption, Phys. Rev. Appl. **18**, 064009 (2022).

[72] D. Kong, X. Hu, L. Hu, and J. Xu, Magnon-atom interaction via dispersive cavities: Magnon entanglement, Phys. Rev. B **103**, 224416 (2021).

[73] D. Kong, J. Xu, Y. Tian, F. Wang, and X. Hu, Remote asymmetric Einstein-Podolsky-Rosen steering of magnons via a single pathway of Bogoliubov dissipation, Phys. Rev. Res. **4**, 013084 (2022).

[74] X. Li, G.-L. Cheng, and W.-X. Yang, Tunable magnon antibunching via degenerate three-wave mixing in a hybrid ferromagnet-superconductor system, Appl. Phys. Lett. **121**, 122403 (2022).

[75] E. Jaynes and F. Cummings, Comparison of quantum and semiclassical radiation theories with application to the beam maser, Proc. IEEE **51**, 89 (1963).

[76] O. Shevchuk, G. A. Steele, and Y. M. Blanter, Strong and tunable couplings in flux-mediated optomechanics, Phys. Rev. B **96**, 014508 (2017).

[77] I. C. Rodrigues, D. Bothner, and G. A. Steele, Coupling microwave photons to a mechanical resonator using quantum interference, Nat. Commun. **10**, 5359 (2019).

[78] M. Kounalakis, Y. M. Blanter, and G. A. Steele, Flux-mediated optomechanics with a transmon qubit in the single-photon ultrastrong-coupling regime, Phys. Rev. Res. **2**, 023335 (2020).

[79] H. Xie, C.-G. Liao, X. Shang, M.-Y. Ye, and X.-M. Lin, Phonon blockade in a quadratically coupled optomechanical system, Phys. Rev. A **96**, 013861 (2017).

[80] Y.-P. Wang, G.-Q. Zhang, D. Xu, T.-F. Li, S.-Y. Zhu, J. S. Tsai, and J. Q. You, Quantum simulation of the fermion-boson composite quasi-particles with a driven qubit-magnon hybrid quantum system, arXiv:1903.12498.

[81] Y.-P. Wang, G.-Q. Zhang, D. Zhang, X.-Q. Luo, W. Xiong, S.-P. Wang, T.-F. Li, C.-M. Hu, and J. Q. You, Magnon Kerr effect in a strongly coupled cavity-magnon system, Phys. Rev. B **94**, 224410 (2016).

[82] Z.-Y. Jin and J. Jing, Magnon blockade in magnon-qubit systems, Phys. Rev. A **108**, 053702 (2023).

[83] H. Carmichael, *Statistical Methods in Quantum Optics* (Springer, Berlin, 1999).

[84] H. Eleuch, Photon statistics of light in semiconductor microcavities, J. Phys. B: At. Mol. Opt. Phys. **41**, 055502 (2008).

[85] M. O. Scully and M. S. Zubairy, *Quantum Optics* (Cambridge University Press, Cambridge, 1997).